

Frontiers of high-tech magnetic materials

H. Kronmüller

Institut für Physik, Max-Planck-Institut für Metallforschung,
Postfach 80 06 65, D-70506 Stuttgart 80, Germany

The discovery of new high-tech magnetic materials sometimes takes place accidentally or by empirical study of a series of alloys and by the interdisciplinary directed collaboration of solid state physicists, chemists and material science engineers. Recent examples for such materials are i) high-coercivity materials based on rare earth-transition metal-metalloid intermetallic compounds with energy products up to 0.4 MJ/m^3 , ii) nanocrystalline high-permeability materials with permeabilities up to $10^5 - 10^6$, iii) giant magnetostrictive alloys of rare earth and transition metals with magnetostrictions up to 1500×10^{-6} . The recent trends in the development of magnetic materials indicate the importance of nanocrystallinity which allows a wide variation of the characteristic properties of the hysteresis loop combined with a more effective use of the intrinsic material parameters.

1. INTRODUCTION

The application of magnetic materials at the beginning of this century was mainly based on carbon steel and the natural iron oxides as magnetite, Fe_3O_4 . As a consequence of the materials quantum theoretical interpretation of spin order by Heisenberg, Bloch and Néel combined with the development of the theory of micromagnetism a more systematic tailoring of magnetic materials has become possible. In particular, the search for high-coercivity, high-permeability, high-remanence, giant magnetostrictive and resistive materials, combined with suitable electrical and mechanical properties, has influenced the field of magnetic materials substantially during the last four decades. Several aspects have to be considered as the origin of this success:

1. The interdisciplinary collaboration between (fig. 1) i) constitution of alloys, ii) microstructure characterization, and iii) the physics of magnetic property \Leftrightarrow microstructure relations.

2. The development of rare earth metal-transition metal alloys or intermetallic compounds.
3. New preparation techniques as liquid phase sintering, melt-spinning, mechanical alloying, multilayer sputtering and molecular beam epitaxy.

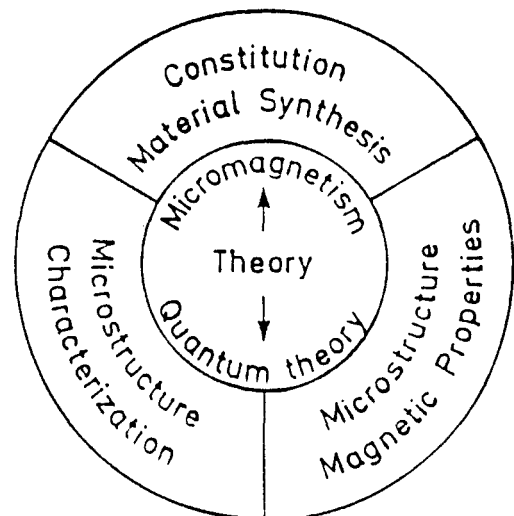


Figure 1. Schematic representation of interdisciplinary collaboration for the development of magnetic materials.

Combinations of these different fields have led to a tailoring of magnetic alloys according to the purpose they are required for.

Transition metals as Fe or Ni in general are the basis for soft magnetic materials whereas alloys of transition and rare earth metals are used for high coercivity materials. Special alloys may be prepared for high density storage or highly magnetostrictive materials.

2. CHARACTERISTIC PROPERTIES OF THE HYSTERESIS LOOP

The fundamental property of magnetic materials is their hysteresis loop and their initial magnetization curve. The hysteresis loop may be characterized by the remanence, M_R , the coercive field, H_c , and its rectangularity. The initial magnetization curve, starting from the fully demagnetized state, in general follow the so-called Rayleigh-law

$$M(H) = \chi_0 H + \alpha_R H^2, \quad (1)$$

which is valid for $H < H_c$. χ_0 denote the initial susceptibility and α_R the Rayleigh constant. These characteristic properties, M_R , H_c , χ_0 , α_R are determined by the intrinsic properties of the magnetic material as spontaneous magnetization, M_S , anisotropy constants, K_1 , K_2 , ..., magnetostriction constants, λ_{ij} , but also by extrinsic properties as the microstructure and the domain pattern. The combination of intrinsic as well as extrinsic properties according to fig. 2 determines the magnetization processes and the characteristic properties of the hysteresis loop.

In all magnetic materials in general a high-remnance is desirable. This holds for electrotechnical applications, for magnetic recording and the sensor technique. In general three groups of elements of the periodic table are important:

1. The magnetic transition metals (TM) Fe, Co, Ni, where Fe and Co in general guarantee large M_S and high Curie temperature.
2. The rare earth metals (RE) are responsible for high magnetocrystalline anisotropies. Especially the light RE metals, but also Dy are of importance.
3. Metalloid elements as B, N or C in amorphous as well as in high-coercivity materials play an important role for improving the intrinsic magnetic and structural properties.

According to these three groups of elements magnetic materials in general are of binary, ternary, quarternary or even higher constitution.

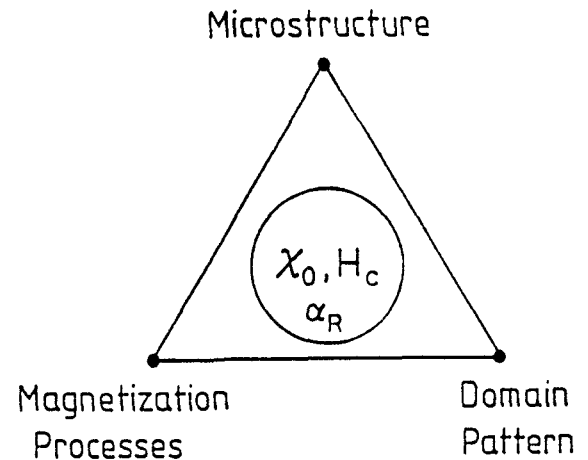


Figure 2. Correlation between magnetic properties, microstructure, domain patterns and magnetization processes.

3. HIGH-COERCIVITY MATERIALS

3.1 Present state of materials development

The coercive field, H_c , is one of the most exciting properties of ferromagnetic materials because its experimental value may vary from several mOe up to 50.000 Oe. This large variation of H_c is

predominantly due to the anisotropy constant, K_1 , which varies from 10^1 (J/m^3) in the case of soft magnetic materials, to several 10^7 (J/m^3) in the case of magnetically hard materials. The general trend of H_c with the anisotropy constant K_1 is shown in fig. 3 for different groups of materials. It turns out that H_c is well described by a general relation [1,2] ($\mu_0 =$ vacuum permeability):

$$H_c = \frac{2 K_1}{\mu_0 M_S} \alpha - N_{eff} M_S \quad (2)$$

Here the first and second term represent modified magnetocrystalline and dipolar magnetic fields, where the parameters α and N_{eff} take care of the deteriorating effects of the microstructure. Eq. (2) has been shown to apply for materials being governed by nucleation as well as domain wall (dw) pinning mechanisms, and also

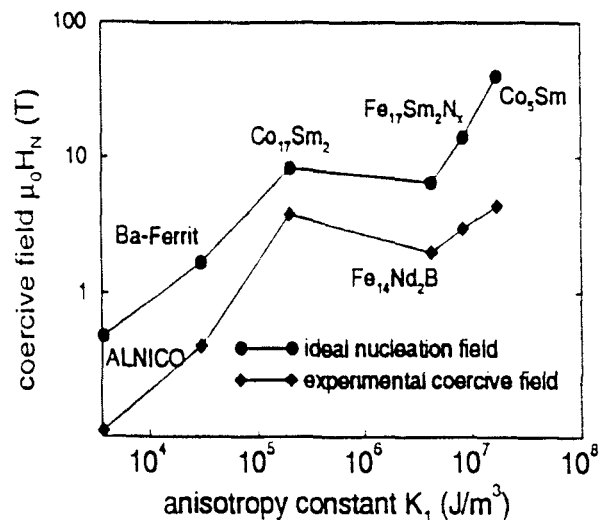


Figure 3. coercive field of prominent magnetic materials as a function of the anisotropy constant K_1 and comparison with $\mu_0 H_c^{theor} = 2 K_1 / M_S$.

the coercive fields of recording media seem to follow eq. (2) [3]. The maximum coercive fields of pms based on intermetallic compounds of RE and TM metals are for Co_5Sm 40 Tesla, for $\text{Co}_{17}\text{Sm}_2$ 9 T, $\text{Fe}_{14}\text{Nd}_2\text{B}$ 6 T, $\text{Sm}_2\text{Fe}_{17}\text{N}_3$ 16 T. Fig. 4 gives a comparison of the experimentally realized coercive fields, H_c^{exp} , with the theoretically expected coercive field $2 K_1 / M_S$ for a series of the most prominent magnets. It is obvious that there exists a large discrepancy of a factor of four between the actual and the theoretical coercive fields. Accordingly the progress in high coercivity materials so far is exclusively due to the discovery of new materials with larger anisotropy constants as demonstrated by fig. 4. Hence, the materials available presently fulfil all intrinsic conditions for high-quality pms, however, the destructive role of the microstructure leads to a limitation of its applicability.

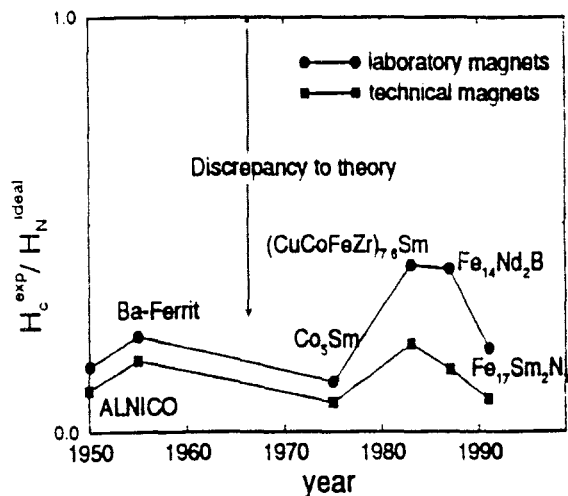


Figure 4. The ratio H_c^{exp} / H_c^{theor} of prominent pms developed during the last four decades (—●— lab. magnets; —■— technical magnets).

3.2 Optimization of microstructures

According to the knowledge accumulated during the last two decades it has become evident that a principal improvement of pms has to start from the creation of an ideal microstructure. Largest coercive fields are obtained for $\alpha \rightarrow 1$ and $N_{eff} \rightarrow 0$. In the case of sintered, rapidly quenched and mechanically alloyed magnets these conditions can only be fulfilled by i) a perfect magnetic decoupling of the individual grains by a nonmagnetic intergranular phase, ii) an ideal alignment of the easy axes, and iii) magnetically perfect grains surfaces. In order to realize all three conditions for grains of average diameters 5 - 20 μm many different production steps have to be taken into account:

1. Choice of a suitable composition of the master alloy in order to avoid precipitation of large nonmagnetic or soft magnetic grains.
2. Choice of suitable additives for enhancing the viscosity of the intergranular nonmagnetic phase, thus guaranteeing an ideal magnetic decoupling between grains.
3. Choice of additives forming small grains of borides within the intergranular phase which act as inhibitors of grain growth during the sintering process.

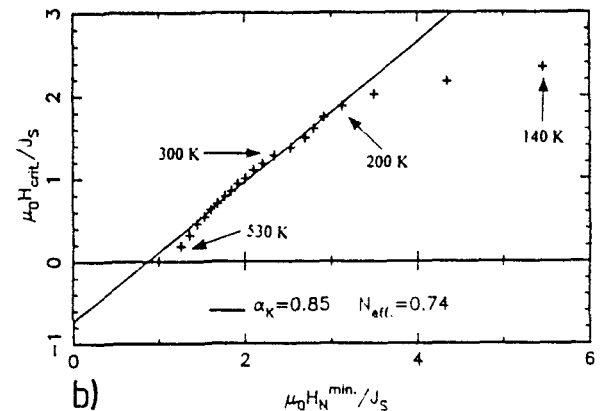
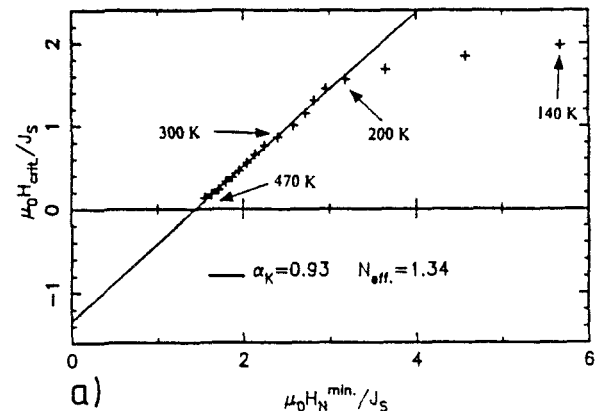
These three aspects require a detailed knowledge of the phase diagram of the ternary or quaternary alloy. As an example we may consider the FeNdB-system. Here an overstoichiometric Nd-content ($\text{Nd}_{18.5}\text{Fe}_{7.5}\text{B}_{6.5}$) guarantees the formation of a two-phase magnet consisting of the hard magnetic phase $\text{Nd}_2\text{Fe}_{14}\text{B}$ and a nonmagnetic Nd-rich intergranular NdFe-alloy.

The viscosity of the Nd-rich alloy may be increased either by Ga [4] or Al [5]. Ga has been proven to be more suitable than Al because it does not dissolve

within the $\text{Nd}_2\text{Fe}_{14}\text{B}$ -phase up to 1.4 % Ga, i.e. it does not reduce the spontaneous magnetization by substituting Fe [6]. As inhibitors of grain growth during the sintering process Nb, Mo and V have been found to be rather effective by forming high-melting borides as, e.g. NbNdB.

3.3 Temperature dependence of H_c

Magnets with the above described additives have been produced by sintering, rapid quenching and mechanical alloying. Coercive fields of 1.6 T - 2.5 T could be realized. In the temperature range from 450 K down to 180 K the temperature dependence of H_c follows eq. (2) (fig. 5a-c). For the analysis α has been factorized according to $\alpha = \alpha_K \alpha_\psi$ (see sect. 3.4) with $\alpha_\psi \sim 0.5$. At lower temperatures the easy directions lie on a cone around the c-axis and eq. (2) has to be modified.



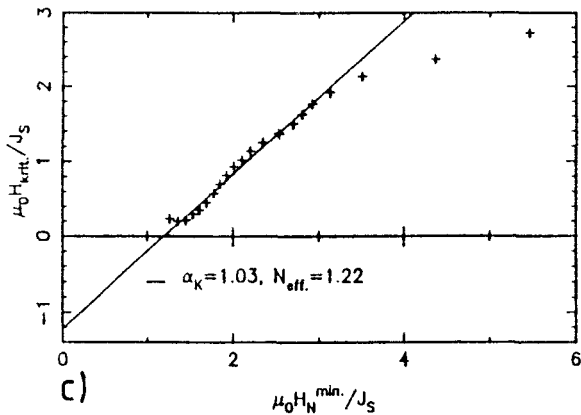


Figure 5. Analysis of the temperature dependence of H_c for different pms using plots H_c / M_S vs. $(2 K_1 / M_S^2) \alpha_\psi$. a) Sintered $\text{Nd}_{18}\text{Fe}_{74}\text{B}_6\text{Ga}_1\text{Nb}_1$ b) Rapidly quenched $\text{Nd}_{18}\text{Fe}_{74}\text{B}_6\text{Ga}_1\text{Nb}_1$. c) Mechanically alloyed $\text{Nd}_{15.5}\text{Fe}_{65}\text{Co}_{10}\text{Dy}_{2.5}\text{B}_{6.25}\text{Ga}_{0.75}$.

In the case of the recently developed nitrated pms of $\text{Sm}_2\text{Fe}_{17}\text{N}_{3-x}$ such a spin rotation does not take place and eq. (2) is found to be valid between 150 K and 480 K (fig. 6). Deviations from eq. (2) at lower temperatures may be due to the not well known temperature dependence of the anisotropy constants [7].

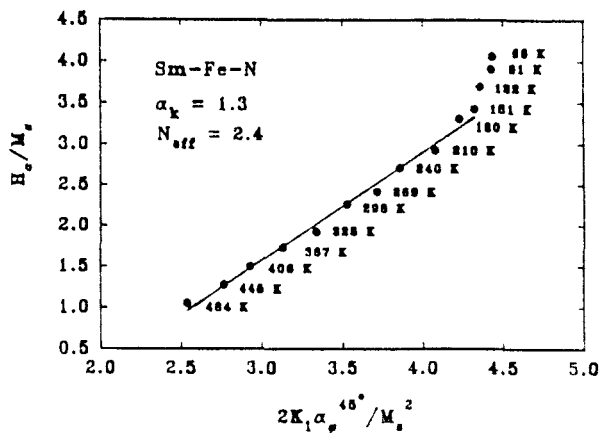


Figure 6. Analysis of the temperature dependence of H_c of $\text{Sm}_2\text{Fe}_{17}\text{B}_{3-x}$.

In all cases analysed so far the parameters α and N_{eff} of eq. (2) are of the order of 0.4 - 0.5 and 0.8 - 3, respectively. Both effects lead to a reduction of H_c by approximately a factor of four.

3.4 Micromagnetic interpretation of microstructural parameters

The unique values found for α and N_{eff} in quite different types of pms point to the fact that there exist principle limits keeping α small and N_{eff} relatively large. For an analysis of α this parameter is factorized according to [2,8]

$$\alpha = \alpha_K \alpha_\psi, \quad (3)$$

where α_K describes the effect of reduced anisotropies at the grain surfaces and α_ψ takes care of the misalignment of the grains's easy axes with respect to the preferred alignment direction of the grains. The value to be taken for the analysis of the temperature dependence of $H_c(T)$, depends exclusively on the microstructure of the material. If the grains are magnetically decoupled the volume average $\langle \alpha_\psi \rangle$ is appropriate. If the grains are strongly coupled by short range exchange interactions and/or dipolar long range interactions the minimum value of α_ψ has to be considered which approximately is given by $\alpha_\psi^{min} = 0.5 (1 + K_2/K_1)$. In sintered and rapidly quenched magnets of $\text{Nd}_2\text{Fe}_{14}\text{B}$ -type magnets α_ψ^{min} has been found to be valid whereas in the case of mechanically alloyed and nitrated magnets of type $\text{Sm}_2\text{Fe}_{17}\text{B}_{3-x}$ the volume average $\langle \alpha_\psi \rangle$ seems to be appropriate.

The large effective demagnetization factors which oftenly exceed the value of $N_{eff} = 1$ are due to strong demagnetization fields at sharp edges and corners of the grains. Especially in the case of sintered and mechanically alloyed pms large values of N_{eff} are found because these production lines favour the formation of polyhedral grains. In the case of

rapidly quenched materials on the other hand small values of N_{eff} but also of α_K are found because of the more spherical grains and more imperfect grain surfaces. This is demonstrated in fig. 7 where the values of α_K and N_{eff} are presented for all types of pms.

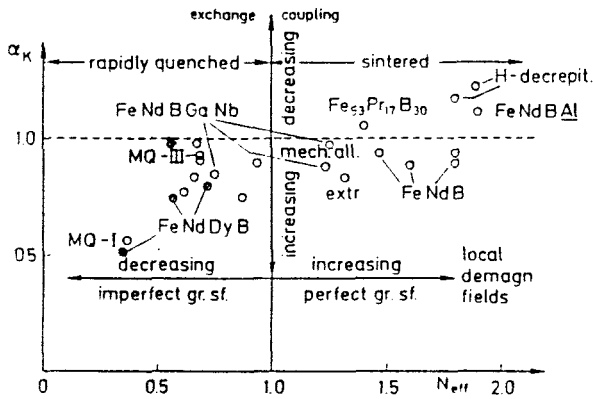


Figure 7. Microstructural parameters α_K and N_{eff} for sintered, rapidly quenched, hot pressed (MQ III) and mechanically alloyed magnets. The trends for increasing exchange couplings and dipolar interaction of the grains are indicated.

It seems to be a general trend that in sintered pms α_K approaches the value 1 thus indicating that the grain surfaces are rather perfect. Unfortunately, the gain in H_c by the large α_K values is lost because N_{eff} increases and compensates the α_K -effect [9]. As mentioned above, the increase of N_{eff} in sintered pms is due to the formation of polyhedral grains with sharp edges and corners. Another effect which is responsible for the low value of $\alpha_K = 0.5$ is the coupling between neighbouring grains by exchange and dipolar interactions which will be considered in the following section.

3.5 Magnetization processes in mesoscopic and nanocrystalline ensembles of grains

According to the analysis of the coercive field misaligned grains are suggested

to be the most effective source in reducing the coercive field. This even seems to be valid for well aligned sintered pms. A micromagnetic prove of this suggestion has been given just recently on the basis of a finite element calculation [10]. Here two cases have been considered: Ensembles of grains with one grain misaligned by 20° where the grains are either coupled by exchange and/or dipolar interactions. In both cases the reversion of magnetization under the influence of a magnetic field starts from the misaligned grain. The critical field for reversion of M_S and the procedure of demagnetization is found to depend on the grain size and the type of coupling.

1. In the case of exchange coupling the entire specimen becomes demagnetized at the reversal of the misaligned grain due to the exchange coupling through the grain boundaries. The spin configuration for zero field around a grain boundary is shown in fig. 8.

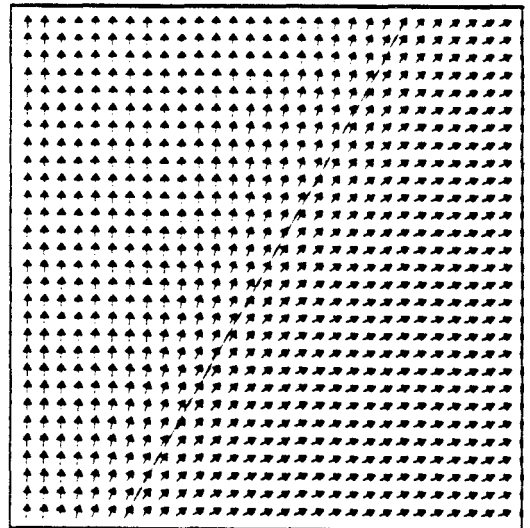


Figure 8. Inhomogeneous magnetic state around a grain boundary due to exchange and dipolar interactions.

Within a region of 4 nm the magnetization approaches the easy axis directions. Therefore, in the case of a misaligned grain with diameter less than 4 nm its deteriorating effect is eliminated by the exchange coupling with the neighbouring grains. In addition, this leads to an enhanced remanence because the well aligned grains now dominate the misaligned grain by exchange coupling. This effect opens the possibility to develop high remanence materials as will be discussed in the following section [11,12].

2. Grains which are coupled only by magnetostatic interactions show a cascade

type demagnetization channel within the grains. Since the range of the demagnetization fields depends on the particle size, large misaligned grains give rise to smaller coercive fields than small grains. This is demonstrated by fig. 9 and fig. 10 where the demagnetization process is presented for average particle sizes of 40 nm and 400 nm. It is evident that in the case of the 400 nm grains the demagnetization process proceeds at much smaller fields than in the case of small grains. As an example we may compare fig. 9 and fig. 10 [13].

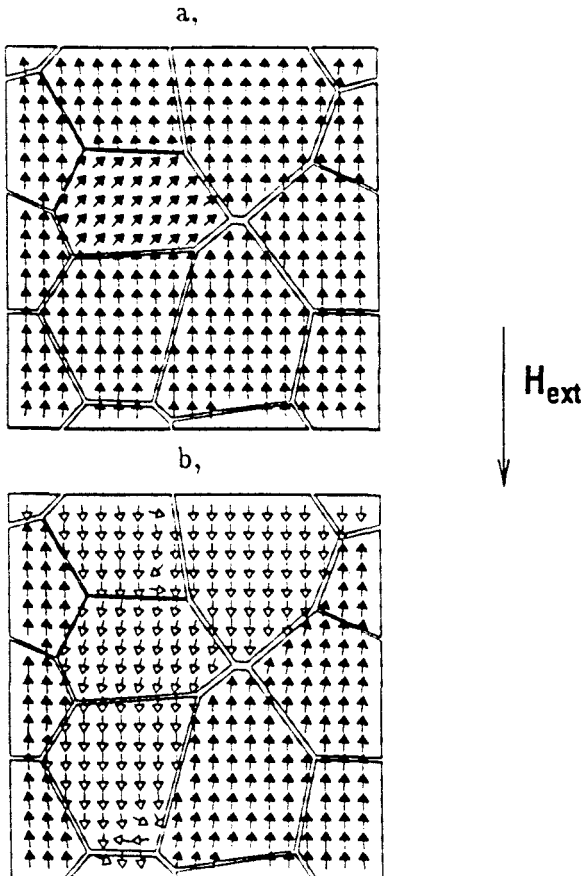


Figure 9. Spin arrangement in an ensemble of grains coupled by dipolar interactions only and containing one misaligned grain (grain diameter 400 nm). a) undercritical state, $\mu_0 H_{ext} = 3.89$ T, b) demagnetization channel for $\mu_0 H_{ext} = 3.90$ T.

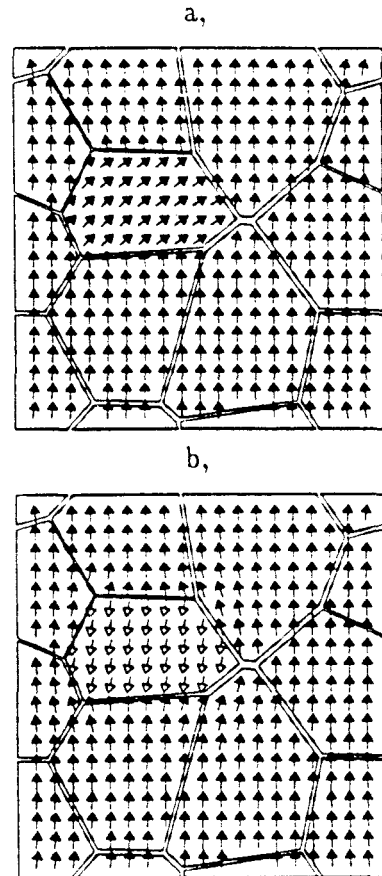


Figure 10. Spin arrangement in an ensemble as in fig. 9 of grains coupled by dipolar interactions only (grain diameter 40 nm). a) undercritical state, $\mu_0 H_{ext} = 4.16$ T, b) localized reversion of the misaligned grain.

In the case of the large grains at a field of $\mu_0 H_{ext} = 3.9$ T four grains around the misaligned grain are reversed whereas in the case of the small grains only the misaligned grain has reversed its magnetization. As a consequence of the long-range dipolar interactions not only the mode of the demagnetization process is influenced but also the absolute value of H_c is considerably reduced. In the case of $Nd_2Fe_{14}B$ considered here the reduction is from 6.8 T to 4.2 T, i.e. a reduction by 40 %. According to these results of a finite element computation the experimental α -values of the order of 0.4 have a natural explanation on the basis of the role of the microstructure. For the production of sintered magnets the following rules can be derived:

1. The grain size in the range above 40 nm has only a minor influence on the coercive field.
2. Magnetic decoupling of the grains by means of additives of Ga, Al, suppresses cascade type demagnetization processes.
3. In sintered pms the grain surfaces are rather perfect due to suitable annealing treatments.
4. Misaligned grains are the most deteriorating source for the coercivity.

3.6 High-remnance exchange-hardened nanocrystalline composite pms

Large energy products, $(BH)_{max} = (1/4) \cdot \mu_0 M_R^2$, in ideal pms are achieved by large remanences, M_R . In a number of papers [12] it has been proposed to produce high remanences by two-phase magnets where one of the phases is α -Fe or Co. These soft magnetic phases may be transformed to become magnetically hardened by means of exchange coupling between the grains. This mechanism becomes effective if the grains have average diameters smaller than twice the wall

width of the hard magnetic phase. In the case of $Nd_2Fe_{14}B$ or $Sm_2Fe_{17}N_{3-x}$ this requires grain sizes below 8 nm. The microstructural and micromagnetic conditions required to produce a high remanence - high coercivity composite material have been investigated by means of micromagnetism and the numerical finite element technique. Two problems have been studied in detail:

1. The effect of grain size.
2. The role of the amount of the soft magnetic phase.

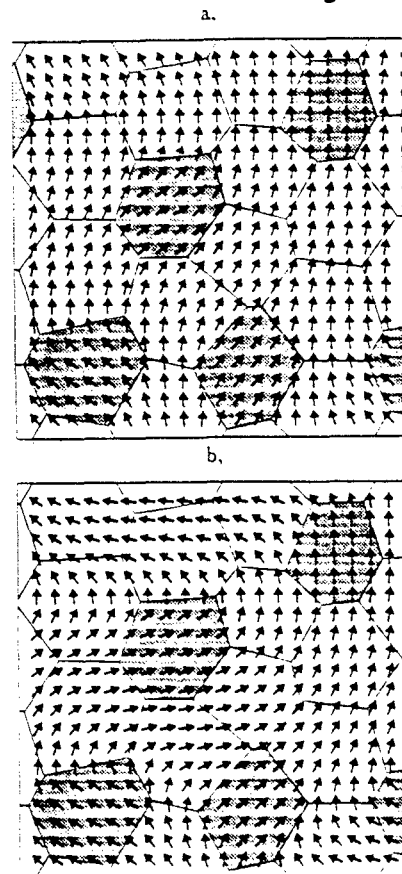


Figure 11. Distribution of spontaneous magnetization in a two-phase magnet in the remanent state for a) $D = 10$ nm and b) $D = 20$ nm. Soft magnetic phase, α -Fe, white and hard magnetic phase, $Nd_2Fe_{14}B$, shaded.

The investigations were performed for the two-phase system $Nd_2Fe_{14}B$ - α -Fe.

These results obtained also should be valid for the two phase system $\text{Sm}_2\text{Fe}_{17}\text{B}_{3-x}-\alpha\text{-Fe}$. The material parameters used for $\text{Nd}_2\text{Fe}_{14}\text{B}$ are $K_1 = 4.3 \cdot 10^6 \text{ J/m}^3$, $K_2 = 0.65 \cdot 10^6 \text{ J/m}^3$, $A = 7.7 \cdot 10^{-12} \text{ J/m}$, $J_S = \mu_0 M_S = 1.61 \text{ T}$ and for $\alpha\text{-Fe}$ $K_1 = 4.67 \cdot 10^4 \text{ J/m}^3$, $K_2 = 2.5 \cdot 10^4 \text{ J/m}^3$, $A = 2.5 \cdot 10^{-11} \text{ J/m}$, $J_S = 2.15 \text{ T}$.

Fig. 11 gives an impression of the distribution of magnetization in a two-phase isotropic magnet (soft magnetic phase 75 %, $\alpha\text{-Fe}$, white grains) with grain sizes of 10 and 20 nm in the remanent state for $H_{\text{ext}} = 0$. The distribution of

magnetization is dominated by the easy directions of the hard magnetic grains (shaded grains). The effect of the exchange coupling on the soft magnetic grains is more pronounced for the 10 nm grains than for the 20 nm grains (fig. 11). This means that in a textured material an enhancement of the remanence takes place. This is demonstrated by the hysteresis loops shown for the first and second quadrants in fig. 12 for the two grain sizes 10 and 20 nm and an increasing amount of the soft magnetic phase.

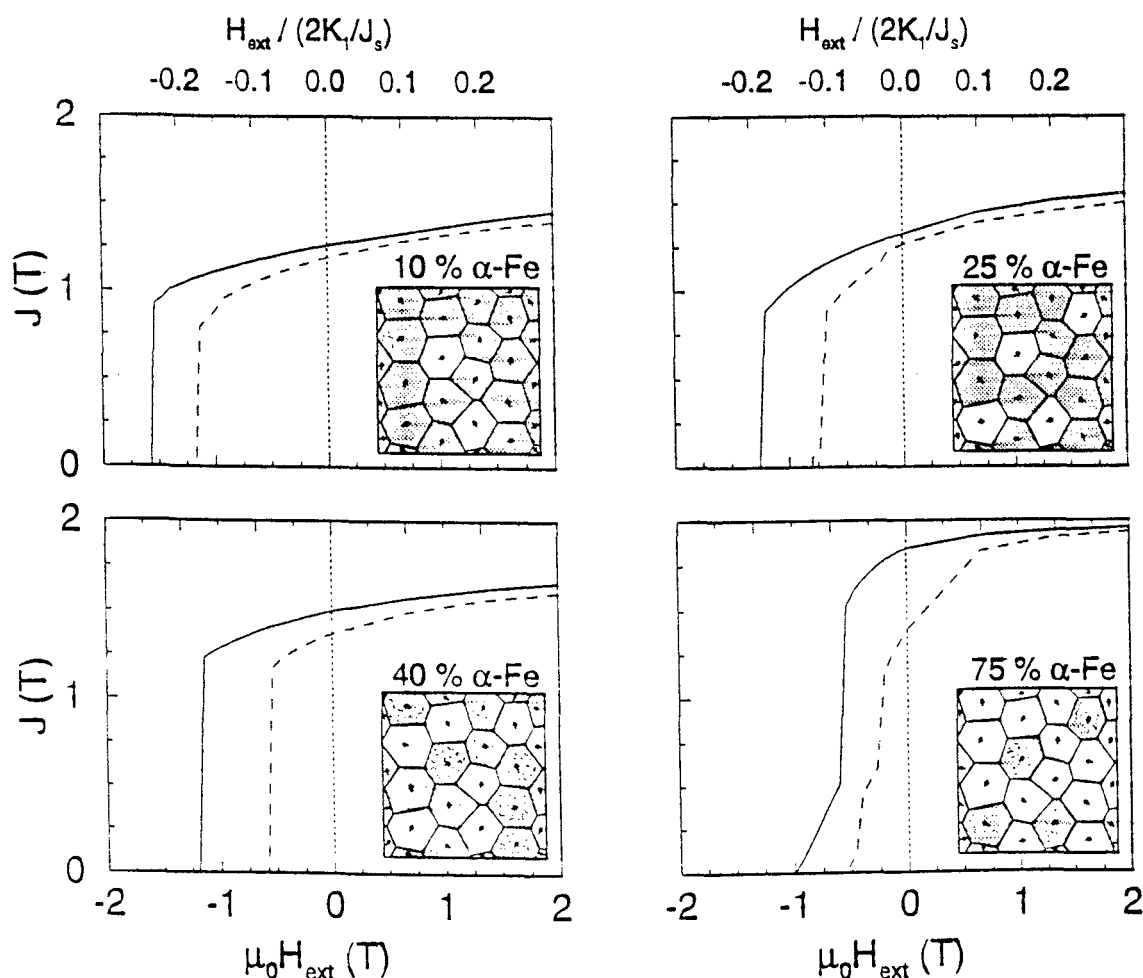


Figure 12. Demagnetization curves of isotropic two-phase pms for different amounts of $\alpha\text{-Fe}$ in $\text{Nd}_2\text{Fe}_{14}\text{B}$. The insets show the grain structure and the arrows indicate the easy axes. White and shaded regions denote soft and hard magnetic phases. The demagnetization curves refer to particles of 10 nm (—) and 20 nm (--).

The following conclusions can be drawn from these model computation:

1. The remanence increases continuously with increasing α -Fe content (fig. 13).
2. The coercive field decreases only moderately with increasing α -Fe content in the case of the 10 nm grains (fig. 13).
3. The energy product $(BH)_{max}$ increases continuously with increasing α -Fe content in the case of the 10 nm grains (fig. 14).

From these results it is obvious that the exchange coupling has the largest benefiting effect in the case of the 10 nm grains. From a technical point of view a composition with 40 % α -Fe seems to give an optimal magnet with a remanence of 1.50 Tesla, a coercivity of 1.25 T, and an energy product of 0.45 MJ/m³. These values may even be improved by introducing a texture by a hot pressing treatment of the nanocrystalline isotropic material.

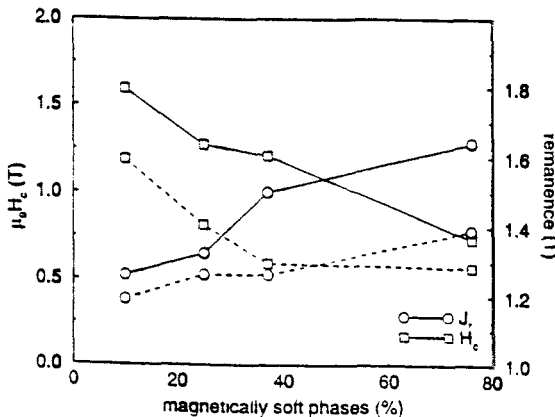


Figure 13. Remanence and coercivity of two-phase pms as a function of the percentage of the magnetically soft phase. Remanence: \circ — \circ 10 nm, \circ --- \circ 20 nm. Coercive field: \square — \square 10 nm, \square --- \square 20 nm.

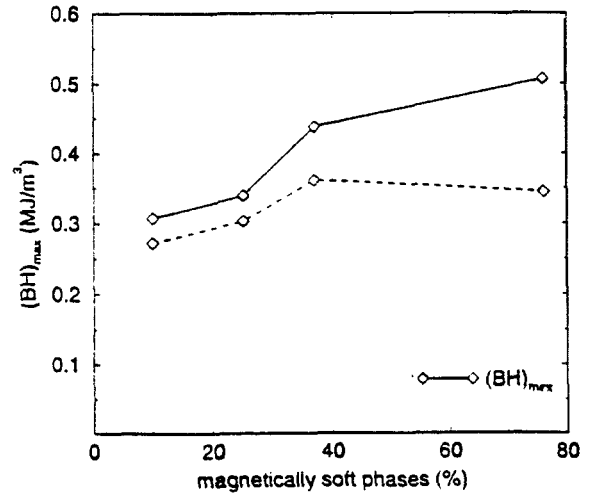


Figure 14. Maximum energy product $(BH)_{max}$ of two-phase pms as a function of the percentage of magnetically soft phase. \diamond — \diamond 10 nm, \diamond --- \diamond 20 nm.

4. NANOCRYSTALLINE SOFT MAGNETIC MATERIALS

4.1 Comparison of amorphous and nanocrystalline materials

Promising materials for future soft magnetic material are the recently developed nanocrystalline iron based alloys [14,15]. These materials are produced by crystallization of initially amorphous alloys. By addition of copper and niobium the basic alloy Fe-Si-B obtains a high nucleation rate and a reduction of the grain growth rate. Well defined grain sizes can be produced by choosing appropriate annealing temperatures and annealing times for the melt-spun amorphous ribbons. As is well known amorphous ferromagnetic alloys are high-permeability materials because of their vanishing magnetic anisotropy and because the magnetoelastic interaction may be eliminated by producing nonmagnetostrictive alloys. In spite of these excellent conditions amorphous alloys at higher temperatures show irreversible structural and magnetic relaxa-

tions. In order to avoid these effects it has been proposed to use nanocrystalline materials which have the advantage to be more stable and also to possess a small electrical conductivity, i.e. small eddy current losses [14,15].

The results obtained for a nanocrystalline ferromagnet of nominal composition $\text{Fe}_{73.5}\text{Cu}_1\text{Nb}_3\text{Si}_{13.5}\text{B}_9$ [16] are shown in fig. 15. Characteristic properties of the initial magnetization curve, χ_0 , H_c , α_R , and the grain size, D , are shown as a function of the annealing temperature. The average grain size varies from 11 to 160 nm in the temperature range between 753 K and 1073 K. As a very surprising result of this annealing treatment it turns out the maximum values of χ_0 and the minimum values of H_c are obtained for the nanocrystalline state at an annealing temperature of $\sim 540^\circ\text{C}$ and a grain size of ~ 13 nm. In a very narrow temperature range from 590 - 620 K χ_0 decreases drastically by more than two orders of magnitude whereas H_c increases by three orders of magnitude. The Rayleigh constant, α_R , decreases by more than six orders of magnitude thus indicating a drastic change of

the type of magnetization processes. As compared to the as-quenched amorphous material the nanocrystalline material has improved χ_0 and H_c by more than a factor of ten.

4.2 Analysis of magnetization processes

The drastic changes of χ_0 and H_c indicate also a change of the type of magnetization processes within the nanocrystalline material. A detailed analysis shows that three types of magnetization processes have to be considered:

1. Domain wall displacements below $T_a = 850$ K ($D < 15$ nm).
2. Rotational processes for 850 K $< T_a < 940$ K (15 nm $< D < 30$ nm).
3. Domain wall bowing for $T_a > 940$ K ($D > 30$ nm).

This interpretation is based on the so-called random anisotropy effect which becomes effective if the grain sizes D are smaller than the exchange length

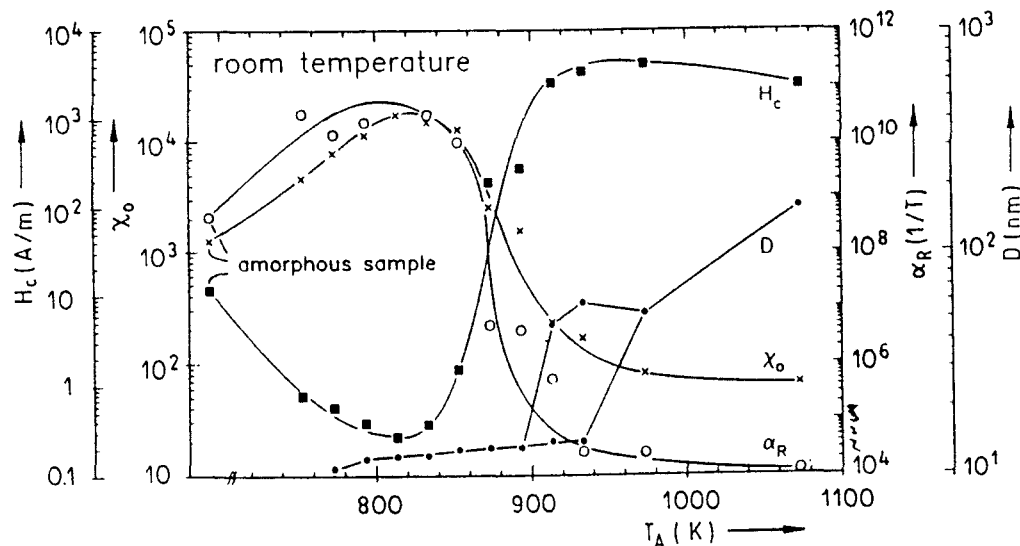


Figure 15. Coercive field, H_c , initial susceptibility, χ_0 , Rayleigh constant, α_R , and grain diameter D of $\text{Fe}_{73.5}\text{Cu}_1\text{Nb}_3\text{Si}_{13.5}\text{B}_9$ as a function of the annealing temperature T_A (annealing time 1 h) [16].

$$l_K = \sqrt{A / K_I} \quad (4)$$

of the nanocrystalline Fe₃Si grains. With the exchange constant $A = 10^{-11}$ J/m, $K_I = 8000$ J/m³, $l_K = 35$ nm is obtained, i.e. l_K is larger than the average grain size for $T_a < 940$ K. In this case the spontaneous magnetization cannot follow the change of the easy directions from one grain to the neighbouring grains. As shown previously the anisotropy constant than has to be replaced by an averaged, effective value [15]

$$\langle K_I \rangle = \frac{K_I^4 D^6}{A^3} \quad (5)$$

As a consequence the domain wall width, $\langle \delta_B \rangle = \pi (A / \langle K_I \rangle)^{1/2}$, extends drastically and for $D = 12$ nm changes from 0.1 μ m to 2.7 μ m. Therefore, in the nanocrystalline material the domain walls average over a large number of grains leading to extremely soft magnetic properties. In order to analyse the magnetization processes we consider the product $\chi_0 H_c / M_S$ which according to fig. 16 varies from $3 \cdot 10^{-3}$ in the amorphous state to approximately 1 in the microcrystalline state. This result now may be analysed on the basis of micromagnetic theories for the different types of magnetization processes [17]:

1. Domain wall displacements

$$\chi_0 H_c / M_S = (3 \cdot \sqrt{\pi} \langle \delta_B \rangle / 4L) \cdot$$

$$[\ln (L / 2 \langle \delta_B \rangle)]^{1/2} = 8 \cdot 10^{-3}$$

(average wall distance $L = 350 \mu$ m,

$$\langle \delta_B \rangle = 2.7 \mu$$
m).

2. Rotational processes

$$\mu_0 H_c = 0.64 \langle K_I \rangle / M_S ,$$

$$\chi_0 = \mu_0 M_S^2 / (3 \langle K_I \rangle) ,$$

$$\chi_0 H_c / M_S = 0.21 .$$

3. Domain wall bowing

$$H_c = 2 \gamma_B / (\mu_0 M_S D) ,$$

$$\chi_0 = (2 \mu_0 M_S^2 / 3 \gamma_B) \cdot (D^2 / L) ,$$

$$\chi_0 H_c / M_S = (4 / 3) (D / L) = 0.026 ,$$

($\gamma_B =$ specific wall energy =

$$4 \sqrt{A \langle K_I \rangle} ,$$

$$D = 40 \text{ nm}, L = 20 \mu\text{m}).$$

The experimental data used for this evaluation have been determined previously [16]. From a comparison of the numerical results for $\chi_0 H_c / M_S$ with the experimental results of fig. 16 it becomes obvious that in the amorphous and nanocrystalline state, $D < 15$ nm, domain wall displacements are active, whereas for $D > 100$ nm the rotational processes are dominant. This also is strongly supported by the drastic decrease of α_R by more than six orders of magnitude.

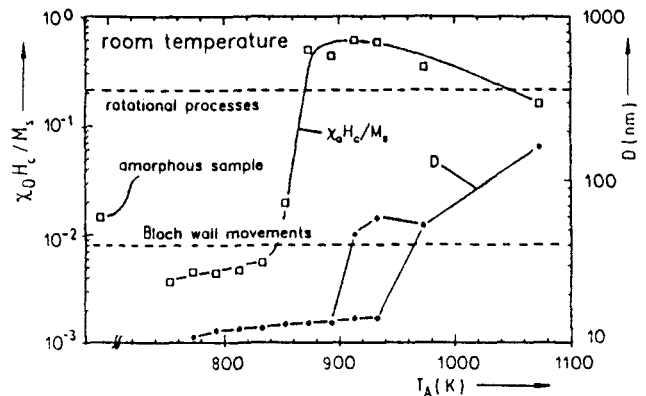


Figure 16. Analysis of magnetization processes by the quantity $\chi_0 H_c / M_S$ as a function of T_A and the grain size D [16].

5. GIANT MAGNETOSTRICTIVE TbDyFe ALLOYS

Giant magnetostrictive alloys may be used for micromechanical applications as for the transformation of electrical signals into mechanical movements. Micro-

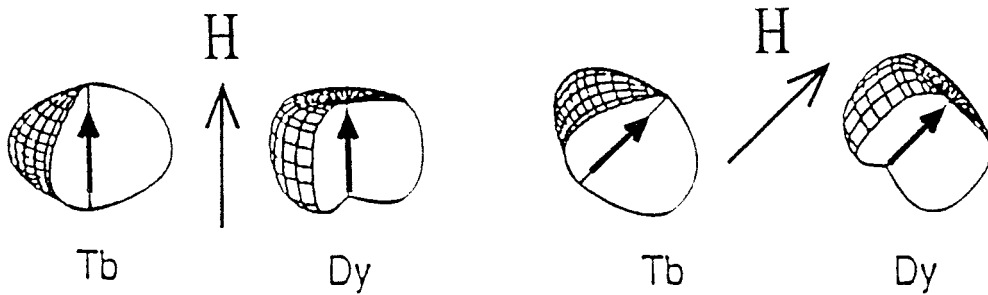


Figure 17. Charge distribution of 4f-electrons in Tb and Dy and rigid rotation due to spin-orbit-coupling.

valves or as elements in integrated electronic circuits in optoelectronics require such actuator-type devices. The alloying system $\text{Tb}_{1-x}\text{Dy}_x\text{Fe}_2$ has been found to be the most suitable system with magnetostrictions up to $\lambda \sim 2.5 \cdot 10^{-3}$ which is a factor of 100 larger than the magnetostriction of TM metals [18]. The large magnetostrictions of the TbFe-based alloys are due to the deformation dependence of the single ion anisotropy of the RE ions. The 4f-electrons of RE ions in general have a rather anisotropic, non-spherical charge cloud as shown in fig. 17 for Tb and Dy. The electrostatic interaction of these charge clouds with the crystal field of the neighbouring ions is responsible for the magnetocrystalline anisotropy energy and also for the magnetostriction. Due to the spin-orbit-coupling the electric charge clouds rigidly rotate under the action of an applied field in the crystal field of the surrounding ions. In the case of the TbDyFe alloys the rotation of the charge cloud is connected with a deformation of the lattice corresponding to a magnetostriction of the order of several 10^{-3} .

For the application of the giant magnetostriction it is necessary that the magnetic saturation is achieved below magnetic fields of 0.1 T. This latter condition requires that the local anisotropy should be as small as possible. In the case of the composition $(\text{Tb}_{0.27}\text{Dy}_{0.73})_{0.43}\text{Fe}_{0.58}$

both conditions, giant magnetostriction and low anisotropy, are excellently fulfilled. For this composition the contributions of Tb and Dy to the anisotropy just compensate each other (oblate + prolate charge distribution, fig. 17). A further reduction of the coercive field is possible by producing amorphous films by the DC-sputter technique [19]. Fig. 18 shows hysteresis loops of an amorphous film of thickness $3 \mu\text{m}$ with the magnetic field applied perpendicular and parallel to the film plane. The coercive fields are below 0.01 T.

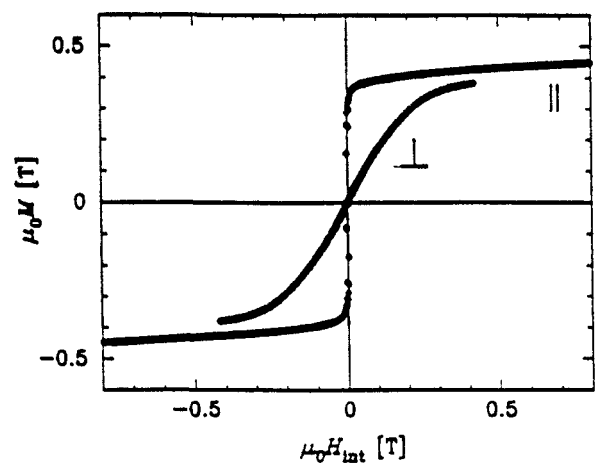


Figure 18. Typical magnetization curves of an amorphous film (20 nm) of composition $(\text{Tb}_{0.27}\text{Dy}_{0.73})_{0.33}\text{Fe}_{0.67}$ [19].

The corresponding magnetization curve of the magnetostriction as shown in fig. 19 clearly shows that 75 % of the saturation magnetostriction is obtained for a field of 0.1 T. Developing nanocrystalline TbDyFe alloys it is expected to obtain even larger saturation magnetostrictions with low effective anisotropies due to the random anisotropy effect.

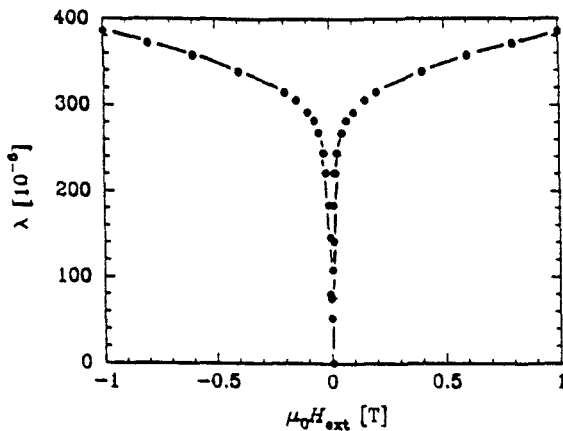


Figure 19. Magnetostriction of an amorphous film of composition $(\text{Tb}_{0.27}\text{Dy}_{0.73})_{0.33}\text{Fe}_{0.67}$ [19].

ACKNOWLEDGEMENT

The author is very grateful to many helpful discussions with Drs. Seeger, Kou and Dipl.-Phys. Schrefl and Bauer.

REFERENCES

1. M. Sagawa and S. Hirosawa, *J. Physique* 49, C8 (1988) 617.
2. H. Kronmüller, K.-D. Durst and M. Sagawa, *J. Magn. Magn. Mat.* 74 (1988) 291.
3. T. Suzuki, H. Notarys, D.C. Dober-
tin, C.-J. Lin, D. Weller, D.C. Mil-
ler and G. Gorman, *IEEE Trans.*
Mag. MAG-28 (1992) 2756.

4. M. Endoh, M. Tokunaga, H. Harada,
IEEE Trans. Mag. MAG-23 (1987)
2290.
5. M. Zhang, D. Ma, X. Jiang, and
S. Liu, *Proc. 8th Int. Workshop on*
RE-Magnets and their Applications,
Ed. K.J. Strnat, Univ. Dayton, 1985,
p. 541.
6. K.G. Knoch, Dr. rer. nat Thesis,
University of Stuttgart, 1990.
7. X.C. Kou, W.J. Qiang, H. Kronmül-
ler and L. Schultz, *J. Appl. Phys.*, to
be published.
8. G. Martinek, H. Kronmüller and
S. Hirosawa, *J. Magn. Magn. Mat.*
89 (1990) 369.
9. H. Kronmüller, *J. Mag. Soc. Japan*
15 (1991) 6.
10. T. Schrefl, H.F. Schmidts, J. Fidler
and H. Kronmüller, *J. Appl. Phys.* 73
(1993) 6510.
11. J. Ding, Y. Liu, P.G. McCormick
and P. Street, *J. Magn. Magn. Mat*
123 (1993) L239; 124 (1993) 1.
12. T. Schrefl, J. Fidler and H. Kronmül-
ler, *J. Magn. Magn. Mat.*, to be
published.
13. H. Kronmüller and T. Schrefl, *Nano-*
magnetic Devices, *Nato Advanced*
Research Workshop, Madrid 1992, to
be published.
14. Y. Yoshizawa and K. Yamauchi,
IEEE Trans. Mag. MAG-25 (1989)
3324.
15. G. Herzer, *IEEE Trans. Mag. MAG-*
26 (1990) 1397.
16. B. Hofmann, T. Reininger and
H. Kronmüller, *phys. stat. sol. (a)*
134 (1992) 247.
17. H. Kronmüller and T. Reininger, *J.*
Magn. Magn. Mat. 112 (1992) 1.
18. A.E. Clark, *Magnetostriction of RE-*
Iron Compounds in Ferromagnetic
Materials, Vol. 1, Ed. E.P. Wohl-
farth, North-Holland Publ. Corp.
Amsterdam 1980, p. 531.
19. F. Schatz, H. Hirscher, G. Flik and
H. Kronmüller, *phys. stat. sol. (a)*
137 (1993) 197.

Curriculum vitae

Full Name: Helmut Friedrich Kronmüller

Date of Birth: November 21, 1931

Personal Status: Married since 1959, 4 children

Citizenship: Fed. Rep. Germany

Educations and Promotions:

- 1959, Dr. rer. nat. thesis, University Stuttgart
- 1968, Dozent of Physics, University Stuttgart
- 1968, Physics Price of German Physical Society
- 1970, Scientific Member of the Max-Planck-Institut für Metallforschung, and Member of the Managing Collegium of the Max-Planck-Institut für Metallforschung
- 1974, Professor of Physics at University Stuttgart
- 1987, Director at the Max-Planck-Institut für Metallforschung

1992, Heyn-Denkmünze of the German Materials
Society

since 1992, Managing Director of the Max-Planck-Institut
für Metallforschung, Stuttgart

